Remote Sensing of Environment 231 (2019) 111224

Contents lists available at ScienceDirect

Remote Sensing of Environment

journal homepage: www.elsevier.com/locate/rse

Extending the SMAP 9-km soil moisture product using a spatio-temporal fusion model

Jiang Hongtao[a], Shen Huanfeng[a,*], Li Xinghua[b], Zeng Chao[a], Liu Huiqin[a], Lei Fangni[c]

[a] School of Resource and Environmental Science, Wuhan University, Wuhan 430079, China
[b] School of Remote Sensing and Information Engineering, Wuhan University, Wuhan 430079, China
[c] USDA ARS Hydrology and Remote Sensing Laboratory, Beltsville, MD 20705, USA

ARTICLE INFO

Edited by Jing M. Chen

Keywords:
SMAP
Radar failure
9-km soil moisture estimation
Spatio-temporal fusion model

ABSTRACT

SMAP satellite has provided us the first 9-km global soil moisture (SM) product, which is retrieved from the combined L-band radiometer and radar observations with a balance between accuracy and resolution. However, SMAP's radar failed on July 7, 2015, making the continuous production of the 9-km SM impossible, which has considerably affected the application of SMAP in hydrological monitoring. This study was aimed at extending the SMAP 9-km SM by developing a non-local filter based spatio-temporal fusion model (STFM). With the auxiliary of the historical 9-kmand 36-km products, the STFM was used to downscale the daily 36-km product to 9-km. Two-year 9-km product was estimated using STFM in the study. It shows that the estimated product has the detailed information retention of 9-km product and the comparable accuracy with 36-km product, which makes it feasible to improve the application potential of the current SMAP SM products.

1. Introduction

The Soil Moisture Active Passive (SMAP) satellite mission developed by the National Aeronautics and Space Administration (NASA) was launched on January 31, 2015. Its aim is to globally measure soil moisture every 2–3 days at a high spatial resolution using the L-band passive radiometer and active radar sensors (Chan et al., 2016; Entekhabi et al., 2010). The significant advantage of this system is the simultaneous acquisition of the L-band radiometer and radar observations, so that the high-accuracy radiometer and fine-resolution radar observations can be effectively combined to derive soil moisture (Das et al., 2011). Three different spatial resolution soil moisture products based on the Equal-Area Scalable Earth 2.0 (EASE2) grid have been released by the SMAP team: 36-km soil moisture (P_{36}) is retrieved only from the SMAP passive radiometer observation; 3-km soil moisture is retrieved only from the SMAP active radar observation; and 9-km soil moisture (AP_9) is retrieved from the combined SMAP active and passive observations. In particular, AP_9 is the first global satellite soil moisture product with a balance between spatial resolution and accuracy. AP_9 can greatly strengthen our understanding of the coupling processes of the terrestrial water, energy, and carbon cycles, improve the capability of flood prediction and drought monitoring, and enhance short-term weather and long-term climate forecasting (Entekhabi et al., 2014b). However, the SMAP radar failed on July 7, 2015, marking it impossible to continue the generation of AP_9, which has seriously affected the application of SMAP in scientific research and hydrological monitoring.

To compensate for the missing AP_9data, the Backus-Gilbert (BG) interpolation method (Backus and Gilbert, 1970) was adopted by NASA to post the microwave polarization brightness temperature (TB) onto the 9-km EASE2 grid. The enhanced SMAP passive 9-km soil moisture product (EP_9) was then retrieved by the interpolated TB using the V-polarized single-channel algorithm (SCA-V) (Jackson, 1993). Although EP_9 enhances the spatial resolution of P_{36}, the richness of the detailed spatial information is far less than that of AP_9, especially in areas with strong spatial heterogeneity. Another solution to extending the fine-resolution soil moisture product was also developed by the SMAP team, where they substituted the SMAP radar L-band observation with the Sentinel-1 synthetic aperture radar (SAR) C-band observation. Thus, the SMAP passive and Sentinel-1 active observations were combined to generate a global soil moisture product with a fine spatial resolution (Das et al., 2016; Lievens et al., 2017; Rudiger et al., 2016; Das et al., 2018). Although the orbit parameters of Sentinel-1 are similar to those of SMAP, and the time difference of the overlapping regions is small, this approach is greatly limited by the narrow bandwidth and long temporal resolution (Das et al., 2016).

The conventional soil moisture downscaling methods can also be used to enhance the spatial resolution of P_{36} and to estimate the 9-km soil moisture. The key idea of these methods is to establish the

* Corresponding author.
E-mail address: shenhf@whu.edu.cn (S. Huanfeng).

https://doi.org/10.1016/j.rse.2019.111224
Received 5 February 2018; Received in revised form 16 May 2019; Accepted 27 May 2019
Available online 13 June 2019
0034-4257/

Table 1
Satellite soil moisture products used in the study.

Product	EASE2 grid	Period	Data level	Method	Auxiliary data[a]
P_{36}	36 km	April 13, 2015–April 12, 2017	L3, Version 4	SCA-V	/
AP_9	9 km	April 13, 2015–July 7, 2015	L3, Version 3	SCA-V	/
EP_9	9 km	April 13, 2015–April 12, 2017	L3, Version 1	BG & SCA-V	/
CD_9	9 km	April 13, 2015–April 12, 2017	/	Piles et al., 2011	P_{36},TB, and MODIS
STF_9	9 km	April 13, 2015–April 12, 2017	/	STFM	P_{36} and AP_9

[a] The data for SCA-V are not listed. Please refer to the SMAP soil moisture product algorithm documentation.

relationship between microwave soil moisture and other high spatial resolution surface parameters, such as land surface temperature (LST) or vegetation indices retrieved from optical/thermal infrared data (Peng et al., 2017; Wang et al., 2016; Sabaghy et al., 2018). In recent years, based on optical/thermal infrared data, a number of scholars have proposed a variety of soil moisture downscaling methods, which have been successfully applied to the Soil Moisture and Ocean Salinity (SMOS) mission, the Advanced Microwave Scanning Radiometer - Earth Observing System(AMSR-E), and so on (Djamai et al., 2016; Jiang et al., 2017; Merlin et al., 2012; Piles et al., 2011; Piles et al., 2016; Sánchez-Ruiz et al., 2014; Song et al., 2014). In terms of SMAP soil moisture, Chen et al. (2017) used a downscaling method to improve the spatial resolution of P_{36} to 250 m, which significantly enriched the detailed spatial information of P_{36}. However, it is very difficult for the conventional downscaling methods to capture the complex relationships between soil moisture and other surface parameters (Peng et al., 2017). Moreover, optical/thermal infrared data are seriously affected by missing information caused by cloud contamination, which poses a great challenge to global 9-km soil moisture estimation.

It should be noted that most of the above methods need other ancillary satellite data (such as SAR data or optical/thermal infrared data). This is not beneficial for estimating soil moisture with a high spatial resolution because of the inherent problems of the ancillary data (e.g., long revisit periods or cloud contamination). Moreover, the historical AP_9 data are not taken into consideration by these methods. As a result of the strong spatio-temporal correlation of soil moisture (Zhang and Chen, 2016; Zeng et al., 2013), the historical AP_9data may be very helpful to estimate the missing 9-km soil moisture. The spatio-temporal fusion model (STFM) can be utilized to fuse the complementary spatial and temporal information of multi-source remote sensing data and to simultaneously estimate remotely sensed data with high spatial and temporal resolutions (Gao et al., 2006; Zhu et al., 2010; Shen et al., 2015; Shen et al., 2016a, 2016b). The STFM has been widely used in the estimation of surface biophysical parameters, such as LST (Shen et al., 2016a, 2016b; Weng et al., 2014; Wu et al., 2015), the normalized difference vegetation index (NDVI) (Meng et al., 2013; Tewes et al., 2015), the leaf area index (Houborg et al., 2016; Zhang et al., 2014), biomass (Dong et al., 2016), and evapotranspiration (Cammalleri et al., 2014; Semmens et al., 2016). Therefore, the STFM provides a new possibility for extending SMAP high-resolution soil moisture, i.e., the use of the STFM for 9-km soil moisture estimation.

In this study, the STFM method is presented to extend the AP_9 product. With the auxiliary of paired baseline data composed of the historical AP_9 and P_{36} data, 9-km soil moisture (STF_9) is estimated based on the corresponding daily P_{36}.One notable advantage of this kind of downscaling method is that it has no need for other ancillary satellite data, which increases the feasibility of continuous production and reduces the possible uncertainty. A two-year period of STF_9products was estimated from April 2015 to April 2017, and these products were validated using the available three months of the original SMAP 9-km product and in-situ data from the International Soil Moisture Network (ISMN) (Dorigo et al., 2011; Dorigo et al., 2013).

2. Data

2.1. Satellite microwave soil moisture

This study deals with the SMAP soil moisture products of P_{36}, AP_9, and EP_9, which have been released by NASA as volume water content (m^3/m^3). The accuracy of $P_{36}$is high in areas where the vegetation water content is $< 5\,kg/m^2$, because TB is only slightly affected by the vegetation and the retrieval error is small (Chan et al., 2016). AP_9 is retrieved from the combined SMAP active and passive observations and makes better use of the advantages of the SMAP L-band in soil moisture monitoring (Colliander et al., 2017; Entekhabi et al., 2014b). Moreover, the detailed spatial information of AP_9 is clearly better than that of P_{36}, which makes it more practical, for applications such as regional-scale agricultural yield estimation, drought monitoring, and soil moisture assimilation. Unfortunately, the SMAP radar failed on July 7, 2015, and NASA was forced to stop production of AP_9. The alternative product, EP_9, released by the NASA SMAP team, is retrieved from the BG-interpolated EASE2 9-km TB using SCA-V. It has been reported that the accuracy of EP_9 is close to that of P_{36} and is better than that of AP_9 (Chan et al., 2017), but the detailed spatial information is clearly weaker than that of AP_9.

In this study, the 9-km soil moisture estimated by the conventional downscaling method (CD_9) (Piles et al., 2011) was used as a comparative dataset for validating the effectiveness of STF_9.The auxiliary data used to estimate CD_9were the Moderate Resolution Imaging Spectro-radiometer (MODIS) LST and NDVI (version 6, global 0.05° MOD11C1 and MOD13C1) and the SMAP 36-km V-polarized TB. The satellite soil moisture products used in this study are summarized in Table 1.

To date, NASA has released SMAP soil moisture products in both ascending and descending nodes, which can be downloaded freely through the National Snow and Ice Data Center (NSIDC). The near-surface temperature homogenization in the morning is better than that in the afternoon, and is thus more conducive to soil moisture retrieval. As a result, the SMAP soil moisture in descending node (06:00 a.m.) is more accurate than that in ascending node (18:00 p.m.) (Burgin et al., 2017). Therefore, only the SMAP soil moisture in descending node was used for the STF_9 estimation. The two study years (Table 1) can be divided into two parts by the failure date of the SMAP radar: the working SMAP radar period T1 (April 13–July 7, 2015) and the SMAP radar failure period T2 (July 8, 2015–April 12, 2017). AP_9 only exists in T1period.The division is made for the following reasons: 1) it allows convenient comparison of the detailed spatial information and accuracy difference between STF_9 and AP_9 (T1period); and 2) it allows us to verify the feasibility of the STFM for long time series STF_9 estimation (T2period).

2.2. In-situ soil moisture

In addition to the evaluation of STF_9 against AP_9in the T1period (before the failure of the SMAP radar), in-situ soil moisture data from the ISMN were also used for accuracy assessment of the T1 and T2 periods. The ISMN is hosted by the Technical University of Vienna and is intended to serve as a centralized data hosting facility where different

in-situ soil moisture networks across the globe are collected. The in-situ soil moisture values were transformed into volumetric units (m^3/m^3) and checked for outliers and implausible values. The in-situ data from the ISMN have been widely used to validate satellite-derived soil moisture and model-simulated or assimilated soil moisture products across the world (Chan et al., 2016; Dorigo et al., 2015; Fascetti et al., 2016; Wu et al., 2016; Zeng et al., 2016). Please refer to Dorigo et al. (2011) and Dorigo et al. (2013) for a detailed description of the ISMN.

In this study, in-situ data from April 13, 2015, to April 12, 2017, were downloaded from the ISMN. The microwave emission measured by the radiometer mostly emanates from the top ~5 cm in the L-band. Only the surface in-situ data (no > 5 cm) from 06:00 a.m. (local time) were utilized to evaluate the satellite-based soil moisture. To allow a better evaluation, the daily P_{36}, EP_9, and in-situ soil moisture should exist at the same time. Furthermore, we set two filtering conditions for the in-situ site selection: 1) the temporal length should be larger than 20 in the T1 period (before the radar failure, April 13, 2015 to July 7, 2015); and 2) the temporal length should be larger than 80 in the T2 period (after the radar failure, July 8, 2015 to April 12, 2017). After screening and merging (where there was more than one in-situ site in the corresponding 9-km pixel), 649 in-situ sites out of 1418 were used to evaluate the gridded soil moisture. A brief introduction to the ISMN soil moisture monitoring networks and the spatial distribution of all the available in-situ sites are provided in Table 2 and Fig. 1, respectively.

3. Method

The purpose of this study was to extend AP_9 using STFM in the case of the SMAP radar failure. As shown in Fig. 2, with the auxiliary of paired baseline data (composed of AP_9 and the corresponding P_{36}in the T1 period), the daily $P_{36}$was input into the model and then the daily $STF_9$was estimated at the corresponding date.

3.1. Composition of the baseline data

As shown in Fig. 2, the ideal baseline data with different spatial resolutions would be P_{36} and AP_9 with a global coverage, so as to estimate STF_9 with the maximum spatial coverage. Considering the short-term stability of soil moisture and the exact 8-day revisit period of SMAP, it should be considered that the 8-day composite can cover the globe. However, there is a difference in spatial coverage for the different 8-day composites in the T1 period. Because surface soil temperature can be < 0 °C or the surface may be covered by snow and ice, there is a lot of uncertainty for soil moisture retrieval (Maitzler, 1994), and SMAP does not carry out soil moisture generation (Entekhabi et al., 2014b). With the failure of the SMAP radar, the available $AP_9$for

Table 2
The maximum, minimum, mean, and standard deviation (SD) of the soil moisture for each ISMN in-situ network (unit: m^3/m^3).

Network	In-situ no.	Max	Min	Mean	SD	Location
BIEBRZA	9	0.600	0.270	0.358	0.082	Poland
COSMOS	40	0.485	0.006	0.184	0.101	USA
FMI	18	0.583	0.001	0.1799	0.099	Finland
HOBE	45	0.494	0.001	0.205	0.083	Denmark
REMEDHUS	20	0.422	0.001	0.132	0.097	Spain
RISMA	22	0.540	0.001	0.257	0.104	Canada
RSMN	11	0.418	0.001	0.162	0.061	Romania
SCAN	118	0.515	0.001	0.178	0.113	USA
SMOSMANIA	17	0.449	0.033	0.208	0.102	France
SNOTEL	214	0.520	0.001	0.185	0.107	USA
SOILSCAPE	45	0.428	0.001	0.150	0.091	USA
TERENO	5	0.456	0.002	0.271	0.090	Germany
UMBRIA	2	0.394	0.161	0.247	0.056	Italy
USCAN	80	0.514	0.001	0.182	0.113	USA
WSMN	3	0.455	0.146	0.291	0.070	UK

composing fine-resolution soil moisture as baseline data covers less than three months (April 13–July 7, 2015). From April to July, the surface soil temperature is on the rise in most areas of the world, and the spatial coverage and the accuracy of SMAP soil moisture are gradually increasing. Experiments have shown that the composite data of the last eight days of the working SMAP radar sensor (June 30–July 7, 2015, T1 period) have the largest spatial coverage of all the continuous 8-day composite data. However, there are some missing data areas for the last 8-day composites, especially for the composited AP_9.To reduce the missing data, the remaining P_{36} and AP_9in the T1 period were used to fill the gaps in the last 8-day composites, respectively. Finally, paired baseline data (Fig. 3) were obtained with the largest spatial coverage.

3.2. The STFM for soil moisture estimation

The STFM has been employed in many different methods and has been widely used for estimating surface parameters with a fine spatial resolution. Inspired by the non-local filter based STFM originally proposed for surface reflectance (Cheng et al., 2017), we present a 9-km soil moisture estimation method by considering the strong spatio-temporal correlation information of soil moisture. In this method, it is assumed that the soil moisture at different spatial resolutions has the same temporal variation. The temporal variation of AP_9 from t_0 day to t_p day can be assumed linearly as:

$$STF_9(x,y,t_p) = a(x,y,\Delta t) * \overline{AP_9}(x,y,t_0) + b(x,y,\Delta t) \quad (1)$$

where $STF_9(x,y,t_P)$ indicates STF_9 at t_P, and $\overline{AP_9}$ indicates the composed AP_9 in the baseline data (Fig. 3b). $\Delta t = t_p - t_0$, t_0 indicates the date of the composed baseline data, t_P indicates the day to be estimated, and $a(x,y,\Delta t)$ and $b(x,y,\Delta t)$ are the linear regression coefficients of pixel (x,y) from t_0 to t_P.

Soil moisture has correlation in the temporal variation information; moreover, it also has strong correlation in the spatial neighborhood information. To make the estimation more accurate, the neighborhood (such as a 5 × 5 window size) similar pixel information is introduced into the estimation process. The so-called similar pixels indicate that the pixels differ from the target pixel (pixel to be estimated) by less than a certain threshold. Please refer to Cheng et al. (2017) for more details about similar pixels. Considering the neighborhood similar pixels, the 9-km soil moisture estimation model is as follows:

$$STF_9(x,y,t_p) = \sum_{i=1}^{n} W(x_i,y_i,t_0) \times [a(x_i,y_i,\Delta t) * \overline{AP_9}(x_i,y_i,t_0) + b(x_i,y_i,\Delta t)] \quad (2)$$

where n, (x_i,y_i), and $W(x_i,y_i,t_0)$ indicate the numbers of similar pixels, the locations, and the weights of similar pixels at t_0, respectively.

However, STF_9 is to be estimated, and it is impossible to select soil moisture similar pixels at a 9-km resolution. To solve this problem, the STFM assumes that the 36-km and 9-km soil moisture products have the same temporal differences. Therefore, the similar pixels of the corresponding position in P_{36} (resampled to 9 km) are used to estimate the regression coefficients and weights. The least-squares regression method is employed to estimate the regression coefficients a and b according to the temporal variation of the neighborhood similar pixels. For the similar pixel weights, taking into account the spatial correlation between similar pixels, the idea of non-local filtering (Buades et al., 2005) is employed for the calculation, as follows:

$$W(x,y,t_0) = \exp\left(-\frac{G * \| \overline{P_{36}}^{\uparrow}(B(x_i,y_i,t_0)) - P_{36}^{\uparrow}(B(x,y,t_p)) \|}{h^2}\right) \quad (3)$$

where $\boldsymbol{G}$ indicates the Gaussian kernel, h indicates the filtering parameter, ↑ indicates the 36-km soil moisture resampled to 9 km using the nearest sampling method, $\overline{P_{36}}$ indicates the composed P_{36} in the baseline data (Fig. 3a), and $B(x_i,y_i,t_P)$ indicates the non-local block **B**

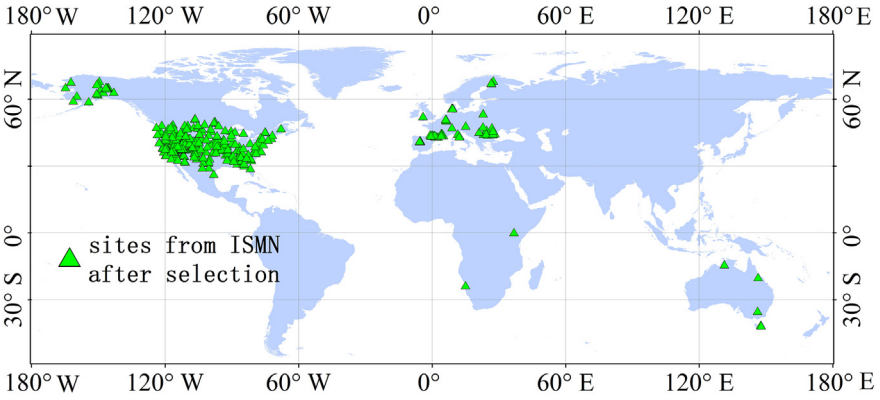

Fig. 1. The 649 in-situ soil moisture sites out of 1418 from the ISMN.

centered at (x_i, y_i).

The STFM assumes the same temporal variation for the 36-km and 9-km soil moisture, so the regression coefficients and weights of the temporal variation are calculated at the 36-km scale and then applied for estimating the 9-km soil moisture using the composed AP_9 in the baseline data (Fig. 3b). There are four processes for estimating daily STF_9 using the STFM: 1) the similar pixels of 9-km resolution at location (x,y) are selected according to the soil moisture at the 36-km resolution; 2) the regression coefficients and the weights of the similar pixels are calculated by the least-squares algorithm and formula (3), respectively; 3) the 9-km soil moisture is estimated by formula (2) at location (x,y) of t_p; and 4) repeat 1)–3) until all the 9-km soil moisture values are estimated at t_p.

4. Results

4.1. Estimated 9-km soil moisture

With the auxiliary of the baseline data (Fig. 3), the missing AP_9could be extended by the STFM using the corresponding daily P_{36} (Fig. 2). It was found that the suitable spatial moving window size for the STFM was 5 × 5 for the 9-km soil moisture estimation. A two-year period of 9-km soil moisture was estimated from April 13, 2015, to April 12, 2017.The estimated soil moisture has been publicly released on http://rs-pop.whu.edu.cn/.The global spatial coverage of the baseline data (Fig. 3) ensures the close spatial coverage for the daily P_{36} and STF_9. Moreover, the SMAP passive observation coverage is clearly larger than its active observation coverage (Entekhabi et al., 2014a), so the AP_9 retrieved from the combined passive and active observations has the same spatial coverage as the SMAP active observation. Therefore, the spatial coverage of the daily STF_9 is close to that of the corresponding daily P_{36}, and should be larger than the daily AP_9.

Fig. 4 shows the spatial distribution of STF_9 in the different seasons of 2016. The spatial distribution of STF_9 is similar to that of P_{36} (Fig. 4); however, the intensity differs greatly in the dense vegetation coverage areas (e.g. the Amazon basin and the Congo basin). This is mainly due to the different spatial distribution between P_{36} and AP_9 (Fig. 3), which is caused by the different surface responses of the SMAP radiometer and the radar observations and the disaggregation method of the SMAP passive TB. Without consideration of the intensity, it can be seen that STF_9 captures the seasonal variation of soil moisture well, and its spatial distribution is consistent with that of P_{36}. This demonstrates the reliability of the STFM for 9-km soil moisture estimation. STF_9obtains more detailed spatial information than P_{36}, which will be beneficial to the practical applications and makes up for the adverse effects brought about by the SMAP radar failure. Notably, there are some missing areas in STF_9 that are inherited from the composed AP_9 (Fig. 3b). The missing areas of STF_9 could be filled by an interpolation method, which will be

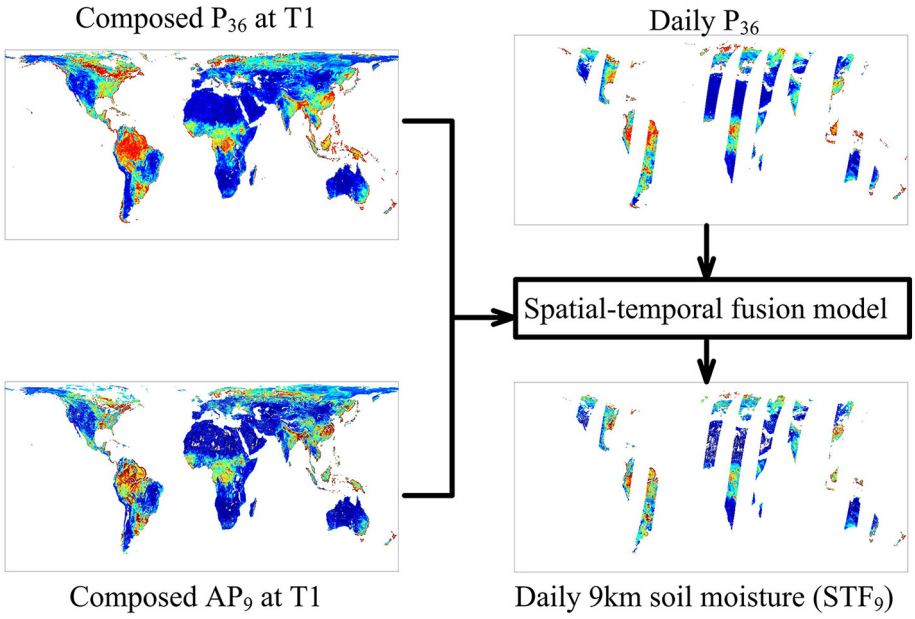

Fig. 2. Flowchart of daily 9-km soil moisture (STF_9) estimation using STFM.

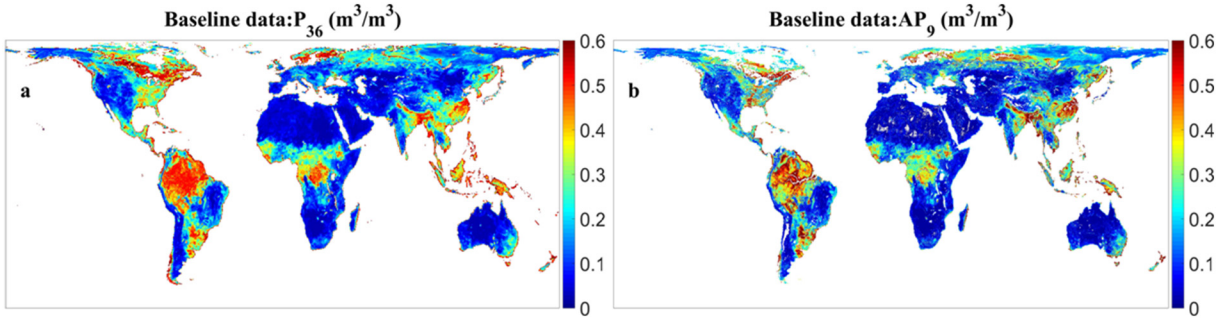

Fig. 3. The baseline data pair composition in the T1period: (a) P_{36} and (b) AP_9.

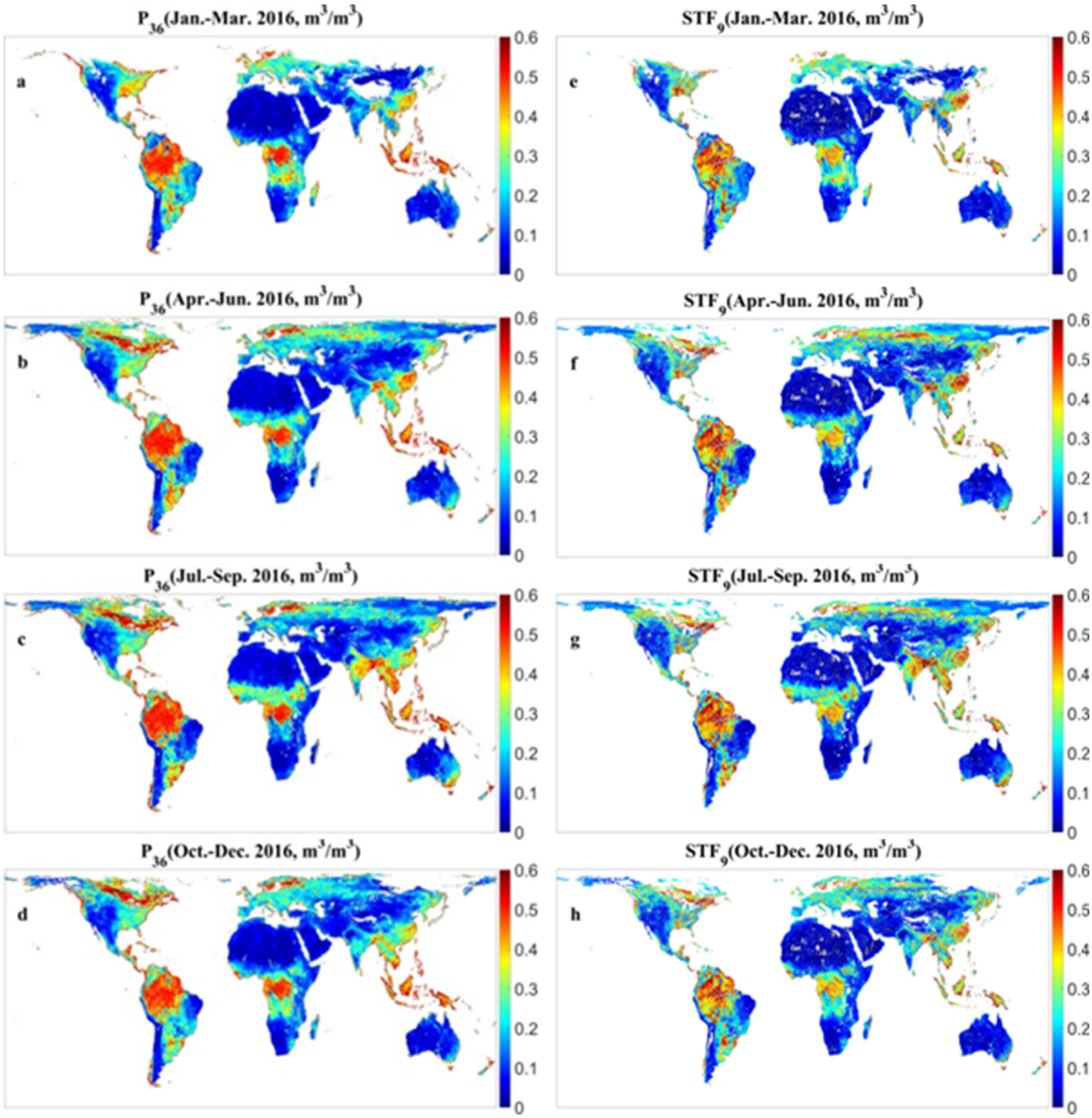

Fig. 4. The spatial distribution of the soil moisture in the different seasons of 2016.

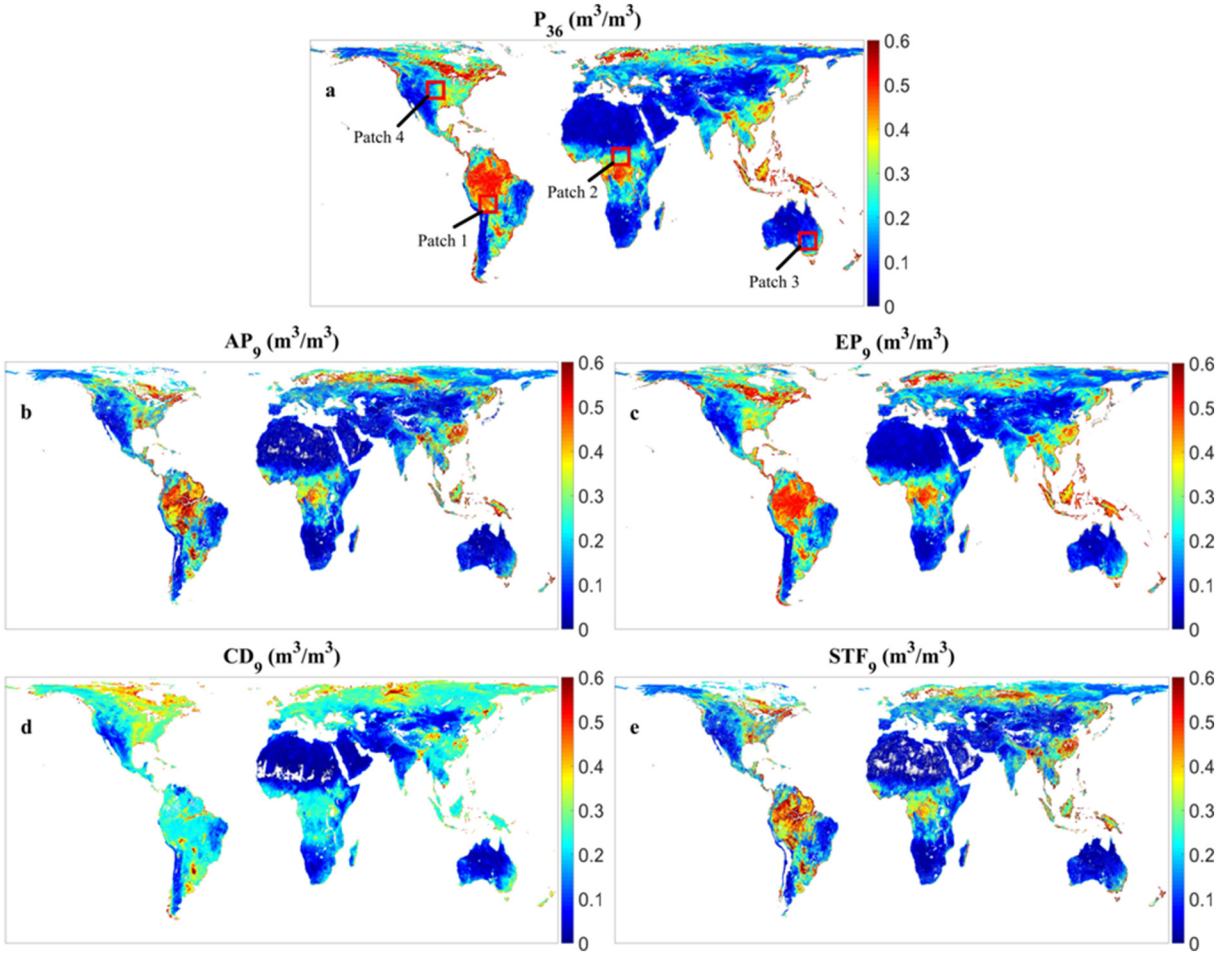

Fig. 5. The 76-day composed (a) P_{36}, (b) AP_9, (c) EP_9, (d) CD_9, and (e) STF_9in the T1period.

addressed in our future study.

4.2. Evaluations

4.2.1. Evaluation before the SMAP radar failure

The 9-km soil moisture estimated by the STFM should have a similar spatial distribution, similar detailed information, and comparable accuracy to AP_9. To compare the difference between AP_9 and STF_9 quantitatively, the last 8-day composed P_{36} and AP_9in the T1 period were used as baseline data, instead of the baseline data shown in Fig. 3, to estimate STF_9. In addition, EP_9 and CD_9were used as comparative datasets to further verify the effectiveness of STF_9.

As the last 8-day composed AP_9 and P_{36}in the T1 period were used as baseline data in the STFM, the remaining 76-day AP_9 data were used as reference to evaluate the difference with STF_9. Fig. 5 shows the spatial distribution of the remaining 76-day composed results of the five soil moisture products (P_{36}, AP_9, EP_9, CD_9, and STF_9) at a global coverage. There is a slight difference between P_{36} and AP_9 (Fig. 5a and b), which is mainly due to the different surface responses of the SMAP radiometer and radar observations and the disaggregation method of SMAP passive TB. In the baseline algorithm of AP_9 retrieval, the TB disaggregation ensures that the TB from the active-passive algorithm is consistent with the radiometer TB, soP_{36} and AP_9 have strong spatial consistency (Entekhabi et al., 2014a, 2014b). Compared with AP_9, the spatial distribution of EP_9 is closer to that of P_{36} because they both use the same microwave polarization TB for soil moisture retrieval (Fig. 5c). CD_9 cannot accurately capture the spatial distribution of P_{36} and AP_9 (Fig. 5d), so there is a big difference. Because the downscaling model cannot accurately simulate the relationship between soil moisture and MODIS data (Peng et al., 2017), it introduces errors while improving the coarse spatial resolution. Moreover, the cloud contamination of MODIS data results in a large amount of missing data for the daily CD_9 (not shown in this paper). Compared to P_{36}, the spatial distribution of STF_9 is much closer to that of AP_9, which meets the expectation of the STFM (Fig. 5e). In general, the spatial distribution of STF_9 is closer to that of AP_9 than EP_9 and CD_9. It is worth noting that the spatial coverage of STF_9 is limited by the 8-day composed AP_9 in the baseline data (Fig. 3b), resulting in less spatial coverage than the 76-day composed AP_9.

Fig. 6 shows the detailed spatial information of the five soil moisture products under different vegetation cover conditions (Fig. 5a, red box areas). The left side of the blue dotted line (Fig. 6) is the SMAP soil moisture, and the right side is the three kinds of 9-km soil moisture. Clearly, the spatial resolution of P_{36} can be improved by all three kinds of 9-km soil moisture. Although the detailed spatial information of EP_9 is somewhat better than that of P_{36}, the richness is far less than that of AP_9. The 9-km TB for EP_9 retrieval is BG-interpolated by the SMAP original passive TB, so the improvement of detailed spatial information is limited. The detailed spatial information of CD_9 is better than that of P_{36} and weaker than that of AP_9. Because the coarse-resolution TB is added into the downscaling model, the promotion of detailed spatial information is limited. The detailed spatial information of STF_9 is very close to that of AP_9 and is clearly better than that of P_{36}, as the estimation of STF_9 takes full account of the temporal and spatial correlation of soil moisture. In general, compared with EP_9 and CD_9, STF_9 demonstrates more detailed spatial information, it shows spatial features more clearly than the others, and it is much closer to AP_9.

The above analysis does not determine the quantitative difference

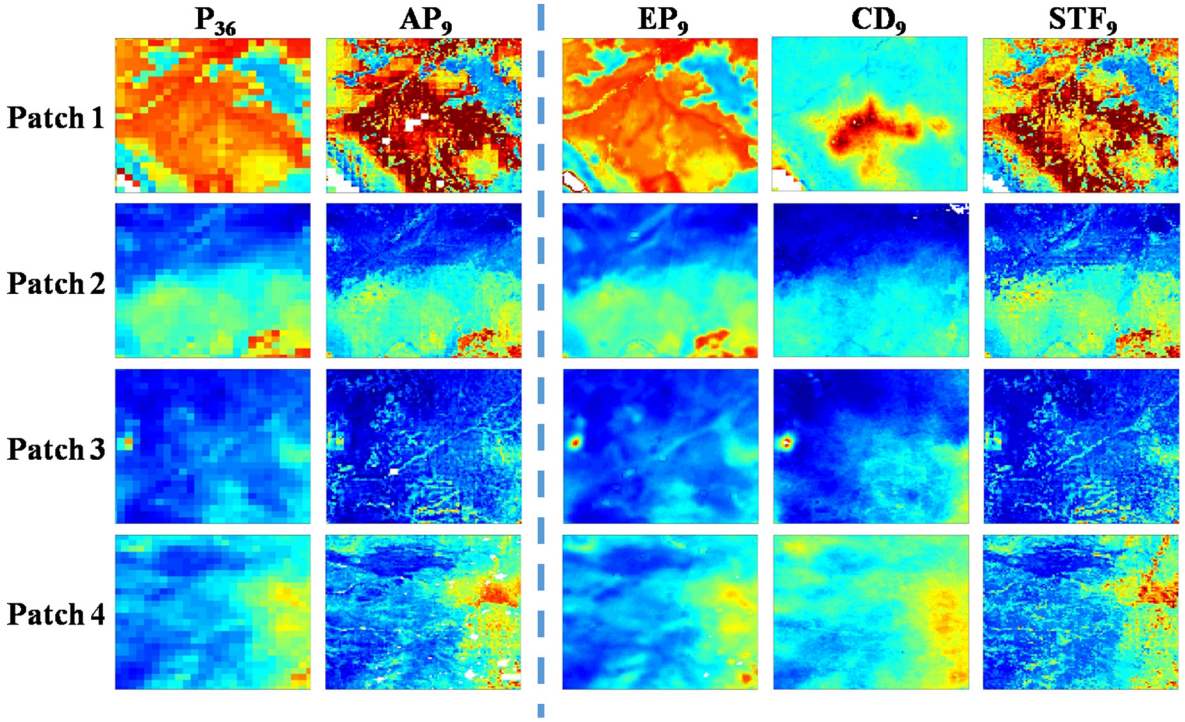

Fig. 6. Detailed spatial information of the five soil moisture products (Fig. 5a, red box areas). The legend is the same as Fig. 5. (For interpretation of the references to colour in this figure legend, the reader is referred to the web version of this article.)

Table 3
Temporal variation of the three kinds of 9-km estimations against AP_9 at the pixel scale (global mean, unit: m^3/m^3).

	R	*bias*	*RMSE*	*ubRMSE*
EP_9	0.637	0.003	0.069	0.040
CD_9	0.422	0.031	0.094	0.049
STF_9	**0.679**	**−0.001**	**0.048**	**0.039**

between the 9-km soil moisture estimates and AP_9. Therefore, the evaluation indices of the correlation (*R*), *bias* (i.e. $STF_9 - AP_9$), root mean square error (*RMSE*), and unbiased *RMSE* (*ubRMSE*) were used to evaluate the temporal variation of the three kinds of 9-km soil moisture at the pixel scale, taking the remaining 76-day AP_9 as reference. The global means of the four indices are summarized in Table 3,and the spatial distribution of *bias* is taken as an example to show the difference between the 9-km soil moisture estimates and AP_9 (Fig. 7).

It can be seen from Table 3 that the evaluation results of the three kinds of 9-km soil moisture against AP_9 are significantly different: the evaluation result of STF_9 is the best, followed by EP_9, and CD_9 is the

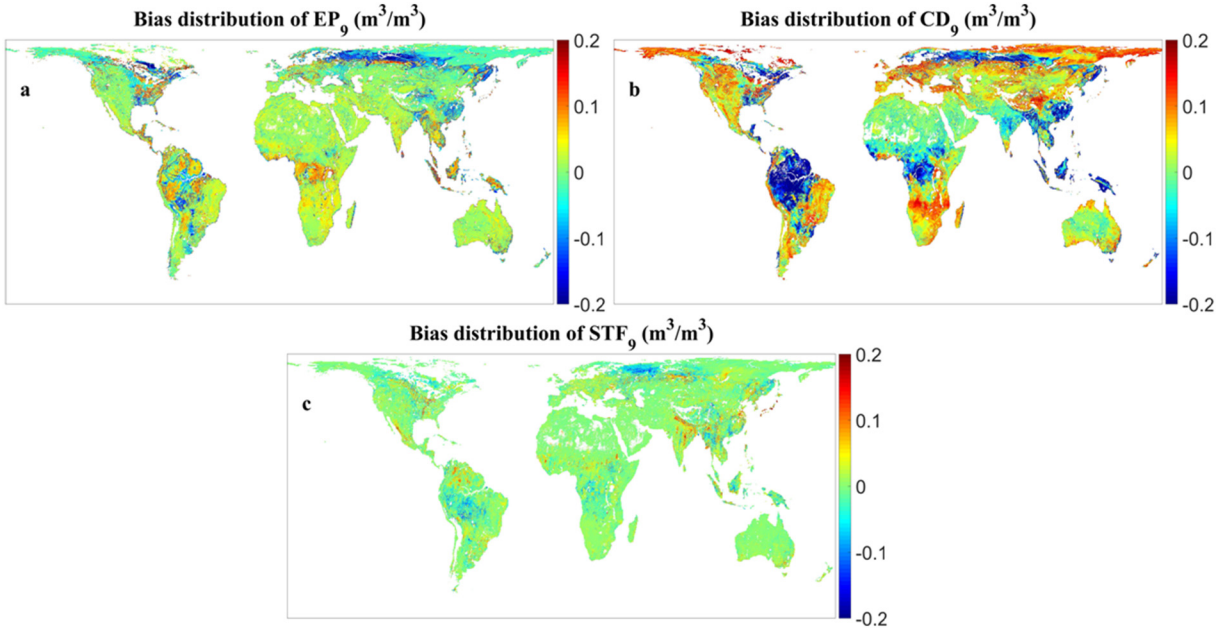

Fig. 7. The *bias* spatial distribution of the three kinds of 9-km soil moisture against AP_9.

worst. The global mean correlation coefficient of STF_9 is 0.679, which is higher than the 0.637 of EP_9 and much higher than the 0.422 of CD_9. This shows that STF_9 can better maintain the temporal variation of AP_9. Moreover, STF_9 has the lowest *bias*, *RMSE*, and *ubRMSE* (indicated by the bold font in Table 3), indicating that its absolute difference with AP_9 is the smallest among the three kinds of 9-km soil moisture. Notably, the *bias* of STF_9 is negative ($-0.001\ m^3/m^3$), indicating the underestimation of AP_9, while the two other methods overestimate AP_9. In brief, STF_9 keeps the temporal variation of AP_9 with the lowest error, confirming the advantage of the STFM for 9-km soil moisture estimation.

From the spatial distribution of the *bias* (Fig. 7), it can be seen that the spatial variability of CD_9 is the strongest, followed by EP_9, and STF_9 is the weakest. The stronger the spatial variability, the greater the difference between the 9-km soil moisture estimate and AP_9, and the greater the difference caused by the estimation model in different regions. EP_9 is retrieved by the BG-interpolated TB and its spatial distribution is consistent with that of P_{36} (Fig. 5). The difference between P_{36} and AP_9 mainly causes the spatial variability of the EP_9*bias* (Fig. 7a). The error of CD_9 is high in dense vegetation coverage and high-latitude areas, which demonstrates the strong spatial variability of the CD_9*bias* (Fig. 7b). There are two reasons for this:1) the accuracy of the soil moisture retrieval is decreased and the NDVI is prone to being supersaturated in the dense vegetation coverage areas, so the downscaling model has less capability in these areas (Piles et al., 2016); and 2) the downscaling model and the SCA-V retrieval model show greater errors during frozen periods (Maitzler, 1994; Sánchez-Ruiz et al., 2014). The spatial variability of the STF_9*bias* is the weakest (Fig. 7c) and the *bias* values are very low in most parts of the world. A possible reason for this is that STF_9 takes full account of the spatial and temporal correlation of the soil moisture, resulting in the estimation being closer to AP_9.Generally speaking, STF_9 is much closer to AP_9 than EP_9 and CD_9 in both temporal variation and numerical value (Table 3 and Fig. 7). The accuracy of the three kinds of 9-km soil moisture with regard to AP_9 is $STF_9 > EP_9 > CD_9$. Therefore, STFM is more suitable for extending 9-km soil moisture than the other two methods.

4.2.2. Evaluation against the SMAP-Sentinel Soil Moisture product and EP_9

The SMAP-Sentinel Soil Moisture (SSSM) product is another possible solution for recovering the missing SAR data. The SSSM product (version 2) has been released by NASA with two kinds of spatial resolution: 3 km and 1 km. The officially released products began in March 31, 2015; however, the amount of data released was very small at the beginning. It was not until the end of 2016 that, mass data release really started. The temporal resolution between SSSM and STF_9 has a great difference. The period of STF_9 covers two years from April 13, 2015 to April 12, 2017, and the period of mass SSSM is from the end of 2016 to date. The time coincidence between the two products is relatively small, so it is difficult to make an effective temporal variation comparison.

The SSSM global product has not yet been released. Fig. 8 shows the global composite of daily 3-km SSSM and the daily STF_9 on April 12, 2017. It can be seen that the spatial distributions of the two soil moisture products are very similar, but the spatial coverage of daily SSSM is far less than that of STF_9. However, the higher spatial resolution of SSSM and the longer temporal resolution make it unsuitable for weather prediction and hydrological motoring.

Table 4
Temporal evaluation result of STF_9against EP_9 and 9 km SSSM (Global mean, unit: m^3/m^3).

	R	RMSE	bias	ubRMSE
EP_9	0.901	0.052	0.001	0.013
9 km SSSM	0.700	0.101	0.003	0.059

At 9kmscale, the EP_9 and SSSM have been demonstrated the similar accuracy against the SMAP core cal/val sites. Therefore, the two years temporal variation of STF_9 is further compared with EP_9 and SSSM which is resized to 9 km scale and is merged globally. As the mass absence of SSSM in global (Fig. 8), the length of temporal variation for STF_9 and SSSM longer than 20 is used for evaluation. As for STF_9 and EP_9, the length of temporal variation is longer than 100. Table 4 shows the evaluations results of STF_9 against EP_9 and 9 km SSSM. It demonstrates that STF_9 has the similar temporal trend with EP_9 and SSSM as the high *R* globally. The small bias and ubRMSE indicate that STF_9 is close to the EP_9 and 9 km SSSM in global scale. The less length of temporal variation results in the more uncertainty of evaluation. Therefore, the evaluation result for EP_9 is better than that of SSSM.

The ubRMSE is computed between STF_9 and the two other SM products at the global extent for each and every valid grid cells at 9 km (Fig. 9). Notably, the length of temporal variation is no < 100 and 20 for EP_9 and SSSM, respectively. Except the dense vegetation covered area, the large amount of ubRMSE between STF_9 and EP_9 is $< 0.02\ m^3/m^3$. It indicates the similar accuracy of EP_9 and STF_9 and can be considered that STF_9 get the good accuracy with detailed spatial information. The difference between STF_9 and SSSM is larger and the absolute difference is larger than $0.02\ m^3/m^3$ in the mass areas. It may be considered that the accuracy slightly differs between STF_9 and SSSM. The good accuracy of SSSM evaluated by the SMAP core cal/val sites, however, the small amount of in-situ data makes the accuracy doubtfully. Furthermore, the other aspect makes the accuracy doubtfully is that the less amount of SSSM data. Nevertheless, it can be considered that the STF_9 can get the good accuracy shown in Table 4 and Fig. 9 in global scale.

4.2.3. Evaluation against ISMN in-situ soil moisture

The 9-km soil moisture estimated by the STFM can capture the detailed spatial information and temporal variation of AP_9 very well; however, the accuracy difference against in-situ data is still unknown. To explore the difference, the two-year period of $STF_9$was estimated by the STFM using the baseline data shown in Fig. 3. The results were then evaluated against ISMN in-situ soil moisture data (Table 2 and Fig. 1). In this way, we could assess the ability of STF_9 for subsequent 9-km soil moisture estimation after the SMAP radar failure. In order to decrease the diversity of more than one in-situ site in the same 9-km soil

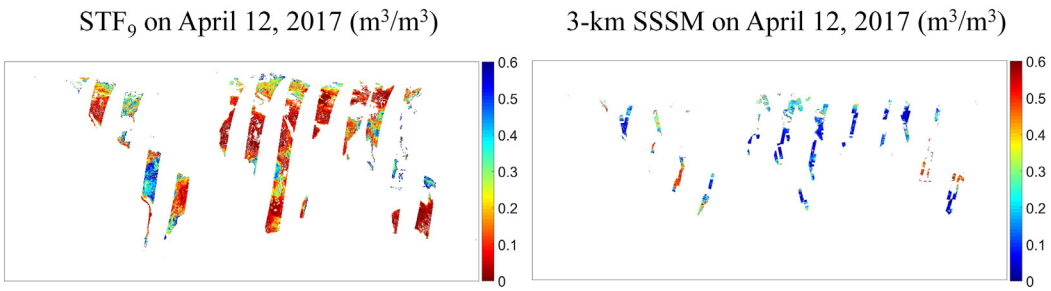

Fig. 8. The spatial distribution of STF_9 and 3-km SSSM on April 12, 2017.

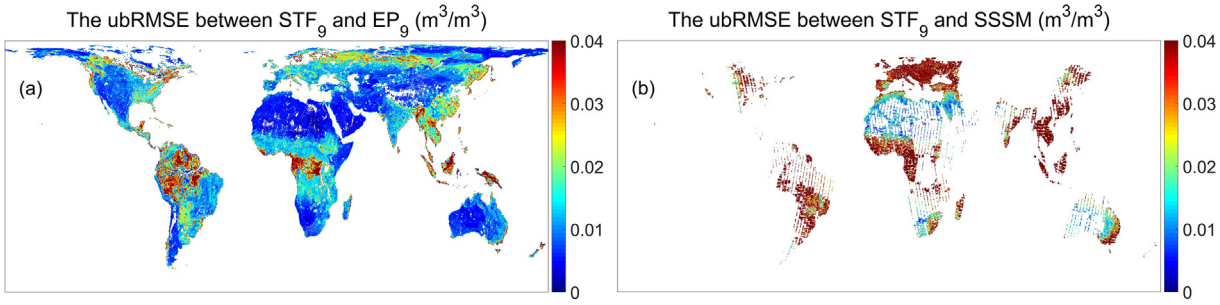

Fig. 9. The ubRMSE between STF_9 and the two other SM products (a: EP_9, b: 9 km SSSM).

Table 5
The average accuracies of the five soil moisture products against ISMN in-situ data.

	R		*bias*(m^3/m^3)		*RMSE*(m^3/m^3)		*ubRMSE*(m^3/m^3)		*P < 0.05*	
	T1	T2	T1	T2	T1	T2	T1	T2	T1	T2
P_{36}	0.575	0.506	−0.032	−0.001	0.101	**0.100**	0.048	0.061	474	619
AP_9	0.427	/	−0.032	/	0.122	/	0.069	/	328	/
EP_9	0.578	0.508	**−0.037**	−0.011	0.102	0.100	0.049	0.062	477	614
CD_9	0.447	0.383	0.030	0.047	**0.099**	0.109	0.053	0.069	359	528
STF_9	**0.580**	**0.512**	−0.034	**−0.001**	0.110	0.108	**0.048**	**0.061**	478	619

Note: the best results are in bold and the second best results are underlined. P < 0.05 indicates the no. of sites with *P*-value < 0.05.

moisture pixel, the arithmetic average of multiple sites of in-situ data was used in the evaluation. The temporal variation validates the accuracy of STF_9, because the in-situ and 9-km soil moisture show some mismatch in spatial resolution and probing depth (Dorigo et al., 2015). The sparse in-situ soil moisture (the ISMN sites used in this study) cannot fully represent the pixel values. Meanwhile, the temporal variation of soil moisture is less affected by the mismatch (Owe et al., 2008). The basic principle of the evaluation is to compare the temporal variation between the in-situ data and the corresponding pixel soil moisture directly, quantified in terms of *R*, *bias* (9-km pixel minus in-situ), *RMSE*, and *ubRMSE*.

Table 5 shows the average accuracies of the five soil moisture products against ISMN in-situ data during the T1 and T2 periods. In fact, it can be seen that the accuracy of AP_9 is less than that of P_{36} (Colliander et al., 2017; Pan et al., 2016), which is validated in the T1 period (Table 5). The accuracy of EP_9 is close to that of P_{36} and is better than that of AP_9, because EP_9 is retrieved by the BG-interpolated 9-kmV-polarized TB and inherits the accuracy of P_{36}. The accuracy of CD_9 is significantly lower than that of P_{36}, is comparable with that of AP_9, and is slightly better than that of AP_9 in some indices such as *RMSE* and *ubRMSE*. However, CD_9 is not estimated in the cloud-contaminated area of the MODIS data, resulting in fewer pixels than AP_9. The accuracy of STF_9 is comparable with that of P_{36} and better than that of AP_9. Among the three kinds of 9-km soil moisture, STF_9 has the highest *R* and *ubRMSE* values (as indicated by the bold font in Table 5), which shows that the STFM can accurately estimate the temporal variation of in-situ soil moisture. Although the *RMSE* and *bias* of STF_9do not show an advantage, this will not affect the accurate application in climate research or weather prediction studies (De Jeu et al., 2014; Dorigo et al., 2012; Liu et al., 2012). The applications do not directly use the absolute value of soil moisture, but instead convert the soil moisture to the range required by the model. Therefore, the relative variations in soil moisture (*R* and *ubRMSE*) are better suited for such applications than absolute variations (*RMSE* and *bias*).

To further compare the accuracies of the three kinds of 9-km soil moisture, their *R* and *ubRMSE* values based on the International Geosphere-Biosphere Program (IGBP) land-cover types in the T2 period are shown in Fig. 10. Except for the evergreen needle leaf forest and savannas, STF_9 has higher *R* values and lower *ubRMSE* values than EP_9 and CD_9in each land-cover type. Nevertheless, the accuracy differences between STF_9 and EP_9 are very small. For CD_9, the accuracies are the lowest in the vast majority of land-cover types. It can be seen that the effect of IGBP land cover on STF_9 is significantly weaker than the effect on EP_9 and CD_9. The reason for this is that the land cover, which is used as the yearly static auxiliary data for SMAP soil moisture retrieval (Entekhabi et al., 2014b), changes only slightly over the two years, so the 9-km soil moisture can be accurately estimated by the STFM.

Although the accuracy of EP_9 is comparable with that of STF_9 (Table 5), the detailed spatial information is clearly weaker than that of STF_9. As a result, STF_9 is more suitable than EP_9 for applications that need strong spatial heterogeneity, such as drought evaluation and prediction, watershed surface runoff estimation, and evapotranspiration studies. The accuracy of $CD_9$is comparable with that of AP_9; however, the spatial distributions differ greatly (Fig. 5). Furthermore, CD_9 is seriously contaminated by cloud and cannot capture the temporal variation of AP_9 very well, which limits the subsequent application as an alternative to AP_9. Overall, among the three kinds of 9-km soil moisture, STF_9 has an unparalleled advantage over EP_9 and CD_9, as STF_9 has a similar spatial distribution and similar detailed information to AP_9 and a comparable accuracy to P_{36}.

4.2.4. Evaluation based on the triple collocation method

The accuracy evaluation against ISMN in-situ soil moisture shows that STF_9 can be considered for the extension of the SMAP 9-km soil moisture product. However, too much uncertainty is brought into the accuracy evaluation, as a result of the big difference between in-situ soil moisture and SMAP pixels in spatial scale. To eliminate the uncertainty, the triple collocation (TC) method was used for the further evaluation of the estimated 9-km soil moisture. The TC method was developed by Stoffelen (1998) to estimate the unknown *RMSE* of three or more linearly-related measurements over the same geophysical variable with mutually independent errors. It also allows the possibility of obtaining the correlation coefficients between the satellite retrievals and the true (but unknown) footprint value (Draper et al., 2013). Therefore, the *R* and *RMSE* were selected as the dominated metrics for the soil moisture evaluation using the TC method.

To estimate the accuracy with the TC method, three kinds of soil moisture products from independent sources are required. Although many kinds of SMAP soil moisture products were used in the study, they are all related to each other. Thus, to use the TC method, the model-

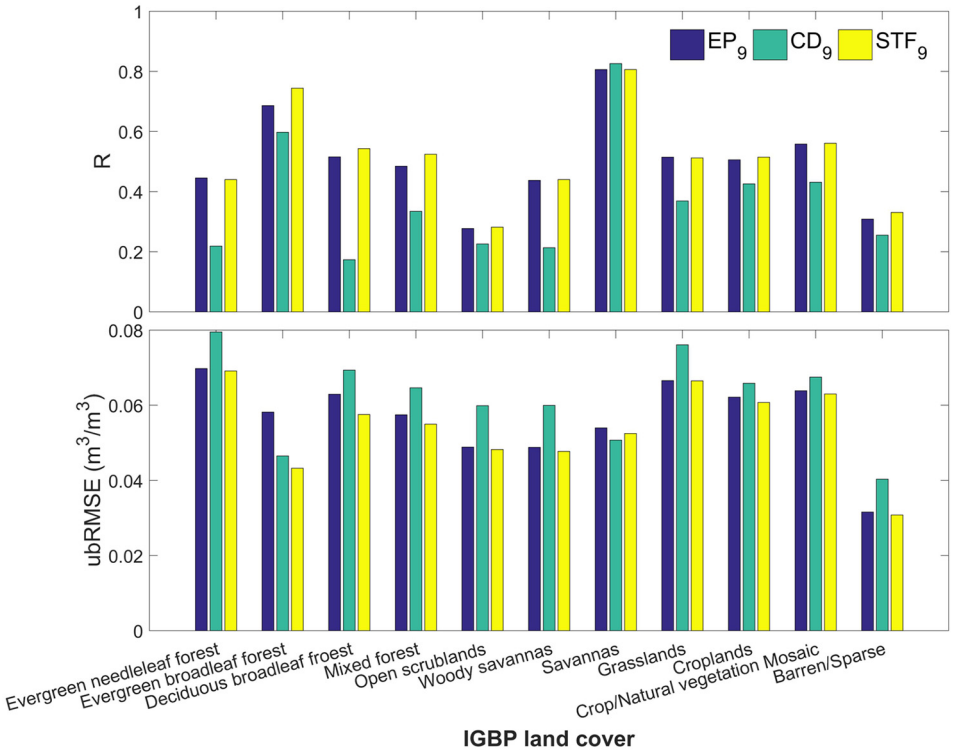

Fig. 10. The average *R* and *ubRMSE* of the three kinds of 9-km soil moisture estimations for each International Geosphere-Biosphere Program (IGBP) land cover in the T2 period.

Table 6
TC evaluations of the two kinds of triplets.

Triplet	In-situ-NOAH-STF_9			In-situ-NOAH-P_{36}		
	In-situ	NOAH	STF_9	In-situ	NOAH	P_{36}
R	0.438	0.808	0.829	0.440	0.809	0.826
RMSE(m^3/m^3)	0.107	0.035	0.034	0.1069	0.035	0.034

Table 7
TC evaluations based on anomaly *R*and *RMSE* for the two kinds of triplets.

TC	In-situ-NOAH-STF_9			In-situ-NOAH-P_{36}		
	In-situ	NOAH	STF_9	In-situ	NOAH	P_{36}
R	0.312	0.703	0.801	0.315	0.700	0.779
RMSE	2.054	0.626	0.586	2.084	0.629	0.593

based surface soil moisture was introduced. This was extracted from the NOAH land surface model (version 2.8), which has been well-evaluated (Ek et al., 2003) and applied in TC application (Hain et al., 2011). Thus, a triplet pattern of in-situ, NOAH, and microwave data was built for the TC evaluation. Two kinds of triplets were constructed—in-situ-NOAH-STF_9 and in-situ-NOAH-P_{36}—so as to compare the temporal accuracy difference between P_{36} and STF_9 from April 13, 2015 to April 12, 2017. Table 6 shows the average TC evaluations of the two kinds of triplets. The *R*and *RMSE* of the in-situ and NOAH data are comparable between the two triplets, which confirm the reliability of TC method for soil moisture evaluation without the ground truth values. The *R*and *RMSE* of the in-situ data are very low, as a result of the big difference between the point scale and the satellite footprint scale. Both the R of STF_9 (0.829) and the R of P_{36} (0.826) are the highest in the each triplet and are very close to 0.83. This confirms the robustness of SMAP for soil moisture retrieval and the comparable accuracy between STF_9 and P_{36}.

As a result of the obvious seasonal variations of soil moisture, the *R* of the temporal variation cannot be used to evaluate precipitation well. This is not conducive to the study of weather and climate change. For this purpose, we further evaluated the variation of the temporal anomaly soil moisture under the framework of the TC method. The method described in Albergel et al. (2009) is used to extract the temporal anomaly soil moisture, and the moving window of the temporal variation was 31 days, 15 days before and after. We stipulated that the temporal anomaly soil moisture was extracted when there were three valid data records in each of the 15 days before and after, and seven valid data records, in total, in the 31-day moving window. According to the pattern of Table 6, Table 7 shows the average TC evaluations of the anomaly soil moisture. The anomaly *R* (Table 7) is less than the *R* shown in Table 6. This phenomenon has been validated in previous works (Zeng et al., 2016; Liu et al., 2012). The anomaly *R* and *RMSE* of $STF_9$are slightly better than those of P_{36}, which suggests that STF_9 is more suitable for the study of weather and climate change. The results confirm that STF_9 has a better accuracy and can better capture the soil moisture. Generally speaking, it can be considered that this further confirms the advantage of STFM for 9-km soil moisture estimation.

5. Discussion

In terms of 9-km soil moisture estimation, the performance of the STFM is clearly better than that of the BG interpolation retrieval method adopted by NASA and the conventional soil moisture downscaling method. This is because STF_9 integrates the respective advantages of the SMAP soil moisture products: the accuracy of P_{36} (Tables 5, 6, and 7) and the spatial resolution of AP_9 (Figs. 5 and 6). The STFM takes full advantage of the temporal and spatial correlation of soil moisture, and only P_{36} and AP_9 are used for estimating the 9-km soil moisture. The method does not require a soil moisture retrieval process or other ancillary satellite data (such as SAR or optical/thermal infrared data), so the error in the 9-km soil moisture estimation process can be decreased. Moreover, there is no time gap between P_{36} and AP_9 as the SMAP passive and active sensors work together on the same satellite

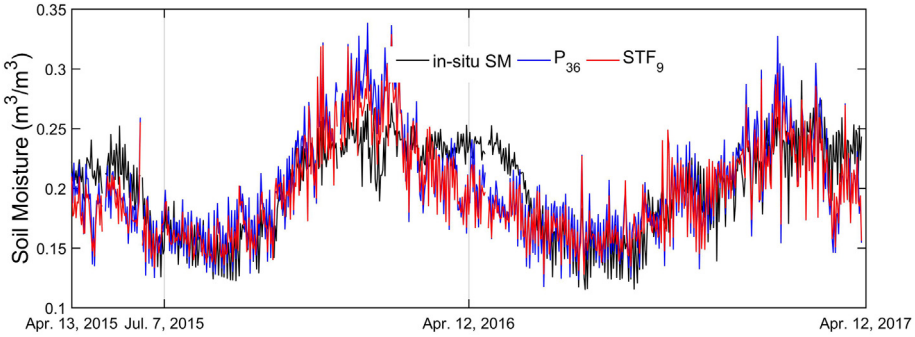

Fig. 11. Temporal variation of the averaged P_{36} and STF_9 based on the in-situ sites from the ISMN.

platform. In comparison, the conventional downscaling method cannot avoid the influence of the time gap because the other ancillary satellite data often have different observation times. As there is no time gap and no other ancillary satellite data requirement for the 9-km soil moisture estimation using the STFM, the error sources of the estimation are decreased and it is a more convenient approach for practical production.

Nevertheless, the uncertainty between P_{36} and the baseline data (Fig. 3) will continue to increase as we move further away from the date of the SMAP radar failure, so it is necessary to discuss its impact on the temporal variation of STF_9. Fig. 11 shows the two-year temporal variation of the averaged P_{36} and STF_9 based on the ISMN in-situ sites. STF_9 is consistent with P_{36}, and the temporal variation is consistent with the in-situ soil moisture. Because there is no significant change in land-cover types over the two-year period, STF_9can maintain the temporal variation of P_{36}. However, there are seasonal differences between P_{36} and STF_9, and the difference between December and January is the most obvious. As the selected ISMN sites are mostly distributed in the northern hemisphere, the probability of SMAP having abnormal soil moisture retrievals increases in winter, which may be the main factor that leads to the obvious difference between STF_9 and P_{36}. Therefore, it is suggested that the seasonal factors may have a greater effect than the distance from the date of the SMAP radar failure in 9-km soil moisture estimation using the STFM in the case of small land-cover changes.

P_{36} underestimates the in-situ soil moisture (negative *bias* in Table 5), which was confirmed in previous studies (Chan et al., 2016; Kim et al., 2017; Zeng et al., 2016); however, the *ubRMSE* of P_{36}in Table 5 does not achieve the expected accuracy of SMAP ($< 0.04\ m^3/m^3$) (Chan et al., 2016) in this study. This is mainly due to the sparse evaluation sites used in the study leading to the larger *ubRMSE* (Dorigo et al., 2015). Only one in-situ site is used in most cases to evaluate the temporal variation of the corresponding 9-km pixel soil moisture. As a result, the large spatial resolution difference between the two kinds of data increases the evaluation error. Furthermore, abnormal value information in the SMAP soil moisture products (Burgin et al., 2017) may be another reason that causes the *ubRMSE* to be on the high side. Although there are some uncertainties in the evaluation against the sparse ISMN in-situ sites, STF_9 keeps the temporal variation of P_{36} very well (Fig. 11). This is the reason why STF_9 inherits the temporal accuracy of P_{36} (Table 5). Moreover, the temporal *R* and *ubRMSE* values of STF_9 are slightly better than those of P_{36} (Table 5), which is determined by the STFM itself. The evaluations using the TC method also confirm that the temporal variation of STF_9 is slightly better that that of P_{36} (Tables 6 and 7). Essentially, the STFM is a kind of filtering algorithm and has a certain smoothing effect (Cheng et al., 2017). For STF_9 estimation, the smoothing of outliers can help to decrease the errors and improve the temporal correlation with in-situ soil moisture. The accuracy of STF_9 is clearly better than that of AP_9 (Table 5), suggesting that the 9-km soil moisture estimated by the STFM will have a wider range of applications. However, only a two-year period of $STF_9$was estimated in this study, and the subsequent estimation results still need further testing and validation.

6. Conclusions

The failure of the SMAP radar has resulted in the unavailability of 9-km soil moisture products. In this study, we adopted the STFM to extend the SMAP 9-km products. The two-year STF_9 products have been publicly released on http://rs-pop.whu.edu.cn/. Compared with other substitute products, i.e., EP_9 and CD_9, the STFM-based STF_9product has an obvious advantage in spatial distribution and detailed information, and is much closer to the original AP_9. The *R* values between AP_9 and EP_9, CD_9, and $STF_9$are 0.422, 0.637, and 0.679, respectively. In addition, the evaluation against ISMN in-situ soil moisture shows that STF_9obtains the best *R* and *ubRMSE* values ($R = 0.667$ and $ubRMSE = 0.048\ m^3/m^3$in the T1 period; $R = 0.598$ and $ubRMSE = 0.060\ m^3/m^3$in the T2 period), performing better than AP_9 and CD_9 and slightly better than P_{36} and EP_9. Furthermore, the evaluations using TC method show that the accuracy of STF_9 is comparable with that of P_{36}. Overall, STF_9 integrates the respective advantages of both SMAP soil moisture products: the high accuracy of P_{36} and the spatial resolution of AP_9. The validation of the two-year products confirmed that the presented method is an effective way to extend the 9-km soil moisture in the case of the SMAP radar failure. However, whether it could be used for the subsequent multi-year data still needs further validation.

Acknowledgment

This research was supported by the Strategic Priority Research Program of Chinese Academy of Sciences (XDA19040504), the National High Technology Research and Development Program (863) of China (2013AA12A301); the National Natural Science Foundation of China (41422108, 41701394); and the Cross-disciplinary Collaborative Teams Program for Science, Technology and Innovation of the Chinese Academy of Sciences. The authors would like to thank the Jet Propulsion Laboratory and NSIDC for making the SMAP data publicly available and the ISMN for providing the *in-situ* data.

References

Albergel, C., R¨udiger, C., Carrer, D., et al., 2009. An evaluation of ASCAT surface soil moisture productswith in-situ observations in southwestern France. Hydrol. Earth Syst. Sci. 13 (2), 115–124.
Backus, G., Gilbert, F., 1970. Uniqueness in the inversion of inaccurate gross earth data. Philos. Trans. R. Soc. A Math. Phys. Eng. Sci. 266, 123–192.
Buades, A., Coll, B., Morel, J.M., 2005. A Non-Local Algorithm for Image Denoising. IEEE Computer Society.
Burgin, M.S., Colliander, A., Njoku, E.G., et al., 2017. A comparative study of the SMAP passive soil moisture product with existing satellite-based soil moisture products. IEEE Trans. Geosci. Remote Sens. 55, 2959–2971.
Cammalleri, C., Anderson, M.C., Gao, F., et al., 2014. Mapping daily evapotranspiration at field scales over rainfed and irrigated agricultural areas using remote sensing data fusion. Agric. For. Meteorol. 186, 1–11.
Chan, S.K., Bindlish, R., O'Neill, P.E., et al., 2016. Assessment of the SMAP passive soil moisture product. IEEE Trans. Geosci. Remote Sens. 54, 4994–5007.
Chan, S.K., Bindlish, R., O'Neill, P., et al., 2017. Development and assessment of the SMAP enhanced passive soil moisture product. Remote Sens. Environ. 204, 2539–2542.

Chen, N.C., He, Y.Q., Zhang, X., 2017. NIR-red spectra-based disaggregation of SMAP soil moisture to 250 m resolution based on SMAPEx-4/5 in southeastern Australia. Remote Sens. (Basel) 9, 51.
Cheng, Q., Liu, H.Q., Shen, H.F., et al., 2017. A spatial and temporal nonlocal filter-based data fusion method. IEEE Trans. Geosci. Remote Sens. 55, 4476–4488.
Colliander, A., Jackson, T.J., Bindlish, R., et al., 2017. Validation of SMAP surface soil moisture products with core validation sites. Remote Sens. Environ. 191, 215–231.
Das, N.N., Entekhabi, D., Njoku, E.G., 2011. An algorithm for merging SMAP radiometer and radar data for high-resolution soil-moisture retrieval. IEEE Trans. Geosci. Remote Sens. 49, 1504–1512.
Das, N.N., Entekhabi, D., Dunbar, R.S., et al., 2016. Uncertainty Estimates in the SMAP Combined Active–Passive Downscaled Brightness Temperature. IEEE Trans. Geosci. Remote Sens. 54, 640–650.
Das, N.N., Entekhabi, D., Dunbar, R.S., et al., 2018. The SMAP mission combined active-passive soil moisture product at 9 km and 3 km spatial resolutions. Remote Sens. Environ. 211, 204–217.
De Jeu, R.A.M., Holmes, T.R.H., Parinussa, R.M., et al., 2014. A spatially coherent global soil moisture product with improved temporal resolution. J. Hydrol. 516, 284–296.
Djamai, N., Magagi, R., Goita, K., et al., 2016. A combination of DISPATCH downscaling algorithm with CLASS land surface scheme for soil moisture estimation at fine scale during cloudy days. Remote Sens. Environ. 184, 1–14.
Dong, T.F., Liu, J.G., Qian, B.D., et al., 2016. Estimating winter wheat biomass by assimilating leaf area index derived from fusion of Landsat-8 and MODIS data. Int. J. Appl. Earth Obs. Geoinf. 49, 63–74.
Dorigo, W.A., Wagner, W., Hohensinn, R., et al., 2011. The international soil moisture network: a data hosting facility for global in situ soil moisture measurements. Hydrol. Earth Syst. Sci. 15, 1675–1698.
Dorigo, W., de Jeu, R., Chung, D., et al., 2012. Evaluating global trends (1988-2010) in harmonized multi-satellite surface soil moisture. Geophys. Res. Lett. 39, 18405.
Dorigo, W.A., Xaver, A., Vreugdenhil, M., et al., 2013. Global automated quality control of in situ soil moisture data from the international soil moisture network. Vadose Zone J. 12, 918–924.
Dorigo, W.A., Gruber, A., De Jeu, R.A.M., et al., 2015. Evaluation of the ESA CCI soil moisture product using ground-based observations. Remote Sens. Environ. 162, 380–395.
Draper C., Reichle R. de Jeu R. et al, ;2013. Estimating root mean square errors in remotely sensed soil moisture over continental scale domains. Remote Sens. Environ. 137: 288–298.
Ek, M.B., Mitchell, K.E., Lin, Y., 2003. Implementation of Noah land surface model advances in the National Centers for Environmental Prediction operational mesoscale Eta model. J. Geophys. Res. Atmos. 108, D22.
Entekhabi, D., Njoku, E.G., O'Neill, P.E., et al., 2010. The Soil Moisture Active Passive (SMAP) mission. P IEEE 98, 704–716.
Entekhabi, D., Das, N., Njoku, E., et al., 2014a. SMAP Algorithm Theoretical Basis Document L2 & L3 Radar/Radiometer Soil Moisture (Active/Passive) Data Products. Revision A, JPL. California Institute of Technology.
Entekhabi, D., Yueh, S., O'Neill, P., et al., 2014b. SMAP handbook. JPL Publication JPL, pp. 400–1567.
Fascetti, F., Pierdicca, N., Pulvirenti, L., et al., 2016. A comparison of ASCAT and SMOS soil moisture retrievals over Europe and northern Africa from 2010 to 2013. Int. J. Appl. Earth Obs. Geoinf. 45, 135–142.
Gao, F., Masek, J., Schwaller, M., et al., 2006. On the blending of the Landsat and MODIS surface reflectance: predicting daily Landsat surface reflectance. IEEE Trans. Geosci. Remote Sens. 44, 2207–2218.
Hain, C.R., Crow, W.T., Mecikalski, J.R., et al., 2011. An intercomparison of available soil moisture estimates from thermal infrared and passive microwave remote sensing and land surface modeling. J. Geophys. Res. Atmos. 116 (D15107).
Houborg, R., McCabe, M.F., Gao, F., 2016. A Spatio-Temporal Enhancement Method for medium resolution LAI (STEM-LAI). Int. J. Appl. Earth Obs. Geoinf. 47, 15–29.
Jackson, T.J., 1993. Measuring surface soil-moisture using passive microwave remote-sensing. Hydrol. Process. 7, 139–152.
Jiang, H.T., Shen, H.F., Li, H.F., et al., 2017. Evaluation of multiple downscaled microwave soil moisture products over the central Tibetan Plateau. Remote Sens. (Basel) 9, 402.
Kim, S.-B., van Zyl, J.J., Johnson, J.T., et al., 2017. Surface soil moisture retrieval using the L-band synthetic aperture radar onboard the soil moisture active–passive satellite and evaluation at core validation sites. IEEE Trans. Geosci. Remote Sens. 55, 1897–1914.
Lievens, H., Reichle, R.H., Liu, Q., et al., 2017. Joint Sentinel-1 and SMAP data assimilation to improve soil moisture estimates. Geophys. Res. Lett. 44, 6145–6153.
Liu, Y.Y., Dorigo, W.A., Parinussa, R.M., et al., 2012. Trend-preserving blending of passive and active microwave soil moisture retrievals. Remote Sens. Environ. 123, 280–297.
Maitzler, C., 1994. Passive microwave signatures of landscapes in winter. Meteorog. Atmos. Phys. 54, 241–250.
Meng, J.H., Du, X., Wu, B.F., 2013. Generation of high spatial and temporal resolution NDVI and its application in crop biomass estimation. Int. J. Digital Earth 6, 203–218.
Merlin, O., Rudiger, C., Al Bitar, A., et al., 2012. Disaggregation of SMOS soil moisture in southeastern Australia. IEEE Trans. Geosci. Remote Sens. 50, 1556–1571.
Owe, M., de Jeu, R., Holmes, T., 2008. Multisensor historical climatology of satellite-derived global land surface moisture. J. Geophys. Res. Earth 113, 196–199.
Pan, M., Cai, X.T., Chaney, N.W., et al., 2016. An initial assessment of SMAP soil moisture retrievals using high-resolution model simulations and in situ observations. Geophys. Res. Lett. 43, 9662–9668.
Peng, J., Loew, A., Merlin, O., et al., 2017. A review of spatial downscaling of satellite remotely sensed soil moisture. Rev. Geophys. 55, 341–366.
Piles, M., Camps, A., Vall-Llossera, M., et al., 2011. Downscaling SMOS-derived soil moisture using MODIS visible/infrared data. IEEE Trans. Geosci. Remote Sens. 49, 3156–3166.
Piles, M., Petropoulos, G.P., Sanchez, N., et al., 2016. Towards improved spatio-temporal resolution soil moisture retrievals from the synergy of SMOS and MSG SEVIRI spaceborne observations. Remote Sens. Environ. 180, 403–417.
Rudiger, C., Su, C.H., Ryu, D., et al., 2016. Disaggregation of low-resolution L-band radiometry using C-band radar data. IEEE Trans. Geosci. Remote Sens. 13, 1425–1429.
Sabaghy, S., Walker, J.P., Renzullo, L.J., et al., 2018. Spatially enhanced passive microwave derived soil moisture: capabilities and opportunities. Remote Sens. Environ. 209, 551–580.
Sánchez-Ruiz, S., Piles, M., Sánchez, N., et al., 2014. Combining SMOS with visible and near/shortwave/thermal infrared satellite data for high resolution soil moisture estimates. J. Hydrol. 516, 273–283.
Semmens, K.A., Anderson, M.C., Kustas, W.P., et al., 2016. Monitoring daily evapotranspiration over two California vineyards using Landsat 8 in a multi-sensor data fusion approach. Remote Sens. Environ. 185, 155–170.
Shen, H.F., Li, X.H., Cheng, Q., et al., 2015. Missing information reconstruction of remote sensing data: a technical review. IEEE Geosci. Remote Sens. Mag. 3, 61–85.
Shen, H.F., Huang, L.W., Zhang, L.P., et al., 2016a. Long-term and fine-scale satellite monitoring of the urban heat island effect by the fusion of multi-temporal and multi-sensor remote sensed data: a 26-year case study of the city of Wuhan in China. Remote Sens. Environ. 172, 109–125.
Shen, H.F., Meng, X.C., Zhang, L.P., 2016b. An integrated framework for the spatio-temporal-spectral fusion of remote sensing images. IEEE Trans. Geosci. Remote Sens. 54, 7135–7148.
Song, C.Y., Jia, L., Menenti, M., 2014. Retrieving high-resolution surface soil moisture by downscaling AMSR-E brightness temperature using MODIS LST and NDVI data. IEEE J. Sel. Top. Appl. Earth Obs. Remote Sens. 7, 935–942.
Stoffelen, A., 1998. Toward the true near-surface wind speed: error modeling and calibration using triple collocation. J. Geophys. Res. Oceans 103, 7755–7766.
Tewes, A., Thonfeld, F., Schmidt, M., et al., 2015. Using RapidEye and MODIS data fusion to monitor vegetation dynamics in semi-arid rangelands in South Africa. Remote Sens. (Basel) 7, 6510–6534.
Wang, J., Ling, Z., Wang, Y., et al., 2016. Improving spatial representation of soil moisture by integration of microwave observations and the temperature–vegetation–drought index derived from MODIS products. ISPRS J. Photogramm. Remote Sens. 113, 144–154.
Weng, Q.H., Fu, P., Gao, F., 2014. Generating daily land surface temperature at Landsat resolution by fusing Landsat and MODIS data. Remote Sens. Environ. 145, 55–67.
Wu, P.H., Shen, H.F., Zhang, L.P., et al., 2015. Integrated fusion of multi-scale polar-orbiting and geostationary satellite observations for the mapping of high spatial and temporal resolution land surface temperature. Remote Sens. Environ. 156, 169–181.
Wu, Q.S., Liu, H.X., Wang, L., et al., 2016. Evaluation of AMSR2 soil moisture products over the contiguous United States using in situ data from the International Soil Moisture Network. Int. J. Appl. Earth Obs. Geoinf. 45, 187–199.
Zeng, C., Shen, H.F., Zhang, L.P., 2013. Recovering missing pixels for Landsat ETM+ SLC-off imagery using multi-temporal regression analysis and a regularization method. Remote Sens. Environ. 131, 182–194.
Zeng, J.Y., Chen, K.S., Bi, H.Y., et al., 2016. A preliminary evaluation of the SMAP radiometer soil moisture product over United States and Europe using ground-based measurements. IEEE Trans. Geosci. Remote Sens. 54, 4929–4940.
Zhang, X., Chen, N., 2016. Reconstruction of GF-1 soil moisture observation based on satellite and in situ sensor collaboration under full cloud contamination. IEEE Trans. Geosci. Remote Sens. 54, 5185–5202.
Zhang, H.K., Chen, J.M., Huang, B., et al., 2014. Reconstructing seasonal variation of Landsat vegetation index related to leaf area index by fusing with MODIS data. IEEE J. Sel. Top. Appl. Earth Obs. Remote Sens. 7, 950–960.
Zhu, X.L., Chen, J., Gao, F., et al., 2010. An enhanced spatial and temporal adaptive reflectance fusion model for complex heterogeneous regions. Remote Sens. Environ. 114, 2610–2623.